Los Alamos NATIONAL LABORATORY EST.1943

LA-UR-15-20135 (Accepted Manuscript)

Synthesis and structure of a stuffed derivative of -quartz, Mg0.5AlSiO4

Xu, Hongwu
Heaney, Peter J.
Yu, Ping
Xu, Huifang

Provided by the author(s) and the Los Alamos National Laboratory (2018-06-14).

To be published in: American Mineralogist

DOI to publisher's version: 10.2138/am-2015-5303

Permalink to record: http://permalink.lanl.gov/object/view?what=info:lanl-repo/lareport/LA-UR-15-20135

Disclaimer:
Approved for public release. Los Alamos National Laboratory, an affirmative action/equal opportunity employer, is operated by the Los Alamos National Security, LLC for the National Nuclear Security Administration of the U.S. Department of Energy under contract DE-AC52-06NA25396. Los Alamos National Laboratory strongly supports academic freedom and a researcher's right to publish; as an institution, however, the Laboratory does not endorse the viewpoint of a publication or guarantee its technical correctness.

RESEARCH LIBRARY

Revision 2

Synthesis and structure of a stuffed derivative of α-quartz, $Mg_{0.5}AlSiO_4$

Hongwu Xu,[1,*] Peter J. Heaney,[2] Ping Yu[3], and Huifang Xu[4]

[1]Earth and Environmental Sciences Division, Los Alamos National Laboratory, Los Alamos, NM 87545

[2]Department of Geosciences, Pennsylvania State University, University Park, PA 16802

[3]Nuclear Magnetic Resonance Facility, University of California at Davis, Davis, CA 95616

[4]Department of Geoscience, University of Wisconsin, Madison, WI 53706

[*]Email: hxu@lanl.gov

Submitted to *American Mineralogist*

March 2015

Always consult and cite the final, published document. See http://www.minsocam.org or GeoscienceWorld

ABSTRACT

A structural derivative of quartz with the composition $Mg_{0.5}AlSiO_4$ has been grown from glass and characterized using synchrotron X-ray diffraction (XRD), transmission electron microscopy (TEM) and ^{29}Si nuclear magnetic resonance (NMR) spectroscopy. Rietveld analysis of the XRD data indicates that the framework of $Mg_{0.5}AlSiO_4$ is isostructural with α-quartz, rather than β-quartz, as is consistent with previous theoretical modeling (Sternitzke and Müller 1991). Al and Si exhibit long-range disorder over the framework tetrahedral sites, indicated by the absence of the superlattice reflections corresponding to the doubling of *c* relative to that of quartz. Nevertheless, ^{29}Si NMR measurements show that Al and Si exhibit partial short-range order with an ordering degree of 56%. Electron diffraction reveals superlattice reflections indicative of doubled periodicities along the *a*-axes. Fourier electron density maps show that Mg occupies channel sites that each are bonded to six O atoms, in contrast to the tetrahedral coordination of Li in the β-quartz-type framework for β-eucryptite, $LiAlSiO_4$. Furthermore, the concentrations of Mg in adjacent channels are different, resulting in framework distortions that generate the superstructures along *a*.

Keywords: Quartz; Eucryptite; Stuffed derivative; Synthesis; Crystal structure; Synchrotron X-ray diffraction; Transmission electron microscopy; Nuclear magnetic resonance spectroscopy

Always consult and cite the final, published document. See http://www.minsocam.org or GeoscienceWorld

INTRODUCTION

As one of the densest framework minerals, quartz has a low tolerance for the incorporation of alien cations into its structure. In natural quartz, there exist only trace amounts (mostly at the levels of hundreds of ppm) of extraneous ions such as Al^{3+}, Fe^{3+} and Na^{+} (Keith and Tuttle 1952; Ghiorso et al. 1979; Smith and Steele 1984), whose concentrations vary with crystallization temperature, solution pH and other formation parameters. Nevertheless, several small cations, including Li^{+}, Mg^{2+}, Zn^{2+}, H^{+} and Na^{+}, can be incorporated within the quartz framework as major component elements when the charge is balanced by the replacement of Si^{4+} cations by Al^{3+} (Müller et al. 1988, 1990; Paulus et al. 1990; Sternitzke and Müller 1991; Palmer 1994; Xu et al. 1999a, 2000; Heaney 2000). The stoichiometric substitution, $Si^{4+} \rightarrow Al^{3+} + M^{+}$ or $\frac{1}{2}\ M^{2+}$ ($M^{+} = Li^{+}$, H^{+}, Na^{+}; $M^{2+} = Mg^{2+}$, Zn^{2+}), results in a series of phases (such as β-eucryptite, $LiAlSiO_4$) that Buerger (1954) classified as "stuffed derivatives of quartz".

Virgilite, $Li_{0.407}(Si_{1.580}Al_{0.400}Fe_{0.013}P_{0.007})O_4$, which occurs in a peraluminous volcanic glass from Macusani, Peru, is the only reported natural occurrence of a mineral with a stuffed quartz structure (French et al. 1978). Though rare in nature, stuffed derivatives of quartz are of considerable interest for their industrial applications (Beall 1994; Müller 1995; Roy 1995). In particular, the so-called LAS (Li_2O-Al_2O_3-SiO_2) phases with compositions $Li_{1-x}Al_{1-x}Si_{1+x}O_4$, $0 \le x < \sim 0.65$, which have the β-quartz structure, exhibit low or even negative coefficients of thermal expansion (CTE) (Xu et al. 2001). As a result, these phases have served as major components of high-temperature glass-ceramic products used in domestic cookware and in many high-precision machines such as jet engines (Beall 1994; Ramalingam and Reimanis 2012). To tailor the thermal

Always consult and cite the final, published document. See http://www.minsocam.org or GeoscienceWorld

properties of LAS phases for specific applications, other small cations, mainly Mg^{2+} and Zn^{2+}, have been used to partially replace Li^{+} (Petzoldt 1967; Beall 1994). Whereas $Zn_{0.5-0.5x}Al_{1-x}Si_{1+x}O_4$, like β-quartz and $Li_{1-x}Al_{1-x}Si_{1+x}O_4$ ($x < \sim 0.65$), exhibits negative CTEs, $Mg_{0.5-0.5x}Al_{1-x}Si_{1+x}O_4$ exhibits positive CTEs (Schreyer and Schairer 1961; Müller et al. 1988; Sternitzke and Müller 1991). This behavior implies that the Mg-stuffed phases may adopt a different structure from β-quartz. However, detailed structural analyses of the $Mg_{0.5}AlSiO_4$–SiO_2 series, including the end member $Mg_{0.5}AlSiO_4$, are scarce, and their structures remain somewhat unclear.

Although an intermediate composition, $MgAl_2Si_3O_{10}$, was studied by single-crystal X-ray diffraction (Schulz 1971; Schulz et al. 1971a, 1971b), its detailed structure was not solved, largely due to the complexities in superperiodicity caused by Al-Si and Mg ordering. Instead, the authors ignored the weak superlattice reflections and determined the average structure of $MgAl_2Si_3O_{10}$ based on a β-quartz-type unit-cell (Schulz et al. 1971b). However, computer modeling using the distance least square (DLS) program demonstrated that this phase has α-quartz-like character in terms of local atomic arrangements, which is presumably responsible for its positive CTEs (Sternitzke and Müller 1991). Thus the true structure of this phase and those of the $Mg_{0.5-0.5x}Al_{1-x}Si_{1+x}O_4$ series in general need further study.

To avoid the complex superstructures and to facilitate comparison with the well-known β-eucryptite ($LiAlSiO_4$), we chose $Mg_{0.5}AlSiO_4$ as a model phase. The sample was synthesized by annealing a glass with the same composition. We analyzed the resulting crystalline phase using powder synchrotron X-ray diffraction (XRD),

Always consult and cite the final, published document. See http://www.minsocam.org or GeoscienceWorld

transmission electron microscopy (TEM), and ^{29}Si nuclear magnetic resonance (NMR) spectroscopy.

EXPERIMENTAL METHODS

Sample synthesis

The $Mg_{0.5}AlSiO_4$ sample was synthesized from glass as follows. First, stoichiometric amounts of $MgCO_3$ (Aesar 99.995%), Al_2O_3 (Aesar 99.99%), and $SiO_2 \cdot nH_2O$ (Fisher) powders were well ground and thoroughly mixed in a mortar. The mixture was transferred to a platinum crucible, melted at 1573 K for ~8 h, and then quenched in air to form a transparent glass. Second, the glass was ground into a powder with a particle size of ~10 μm. This powder was then heat-treated at 1173 K for ~7 h in a muffle furnace. The resulting product was a white, well-crystalline single-phase, as revealed by XRD (see below).

Because the $Mg_{0.5}AlSiO_4$ stuffed-quartz phase is thermodynamically metastable (Strnad 1986), its crystallization from the $Mg_{0.5}AlSiO_4$ glass required the bracketing of annealing temperatures and times. Higher temperatures and/or longer times resulted in the formation of stable phases, such as cordierite and cristobalite, whereas lower temperatures and/or shorter times yielded samples with poor crystallinity. Our crystallization parameters, 1173 K and ~7 h, were determined after a number of trial syntheses at other conditions. Syntheses of quartz solid solutions in the MgO-Al_2O_3-SiO_2 system by other researchers frequently employed TiO_2, ZrO_2 or their mixtures as nucleating agents to facilitate the crystallization (Strnad 1986). To prepare a phase-pure $Mg_{0.5}AlSiO_4$ sample for the purpose of detailed structural analysis, we did not use any

Always consult and cite the final, published document. See http://www.minsocam.org or GeoscienceWorld

nucleating agents. Nevertheless, excellent crystallinity of our synthesized $Mg_{0.5}AlSiO_4$ sample was achieved.

Transmission electron microscopy (TEM)

Specimens for the TEM studies were prepared by grinding the synthesized $Mg_{0.5}AlSiO_4$ sample with ethanol in an agate mortar and placing a drop of the suspension on a holey-carbon grid. Selected-area electron diffraction (SAED) and energy-dispersive spectroscopy (EDS) were conducted with a JEOL 2010 microscope equipped with an Oxford- Link ISIS EDS system and operated at 200 keV. Quantitative analyses of EDS spectra were carried out using k-factors obtained from forsterite and anorthite standards.

NMR spectroscopy

The ^{29}Si magic angle spinning - nuclear magnetic resonance (MAS-NMR) spectrum of $Mg_{0.5}AlSiO_4$ was acquired using a Bruker AVANCE 500 spectrometer equipped with an 11.74 T wide-bore magnet. The ^{29}Si Larmor frequency was 99.35 MHz. Sample powders were held in a zirconia rotor (with an outside diameter of 4 mm) spinning at 7 kHz. A single pulse of 1 μs (corresponding to a tip angle of 30^o) with a recycle delay of 60 s was used for excitation. The chemical shift was externally referenced to the standard tetramethylsilane (TMS).

Powder synchrotron X-ray diffraction and Rietveld analysis

Powder XRD measurements were carried out with a linear position-sensitive detector (PSD) at beam line X7A of the National Synchrotron Light Source (NSLS), Brookhaven National Laboratory (BNL). The wavelength used was 0.700789 Å, as calibrated with a CeO_2 standard. Sample powders were sealed in a silica-glass capillary of 0.02-mm diameter, and to minimize preferred orientation, the capillary was rocked

Always consult and cite the final, published document. See http://www.minsocam.org or GeoscienceWorld

through ±10° during data collection. Data were collected from 7° to 55° 2θ in the step-scan mode using step sizes of 0.25° and counting times of 10 s (7–15°), 20 s (15–30°), 40 s (30–45°), and 80 s (45–55°) per step.

The synchrotron XRD data were analyzed by the Rietveld method with the General Structure Analysis System (GSAS) program of Larson and Von Dreele (2000). The starting parameters for the basic β- and α-quartz-type structures were taken from the studies of $MgAl_2Si_3O_{10}$ (Schulz et al. 1971b) and α-SiO_2 (Will et al. 1988), respectively. As described below, our final refined structure was based on an α-quartz-like superstructure with doubled periodicities along the **a**-axes. Our refinements proceeded as follows: after the scale factor and four radial distribution function (RDF) background terms (needed to model the background from the capillary glass) had converged, specimen displacement and lattice parameters were added and optimized. Sixteen additional background terms were then added, and the peak profiles were fitted by refining isotropic and anisotropic broadening parameters and a Gaussian particle size coefficient in a pseudo-Voigt function (Thompson et al. 1987; Cox et al. 1988; Finger et al. 1994). On convergence of the preceding parameters, atomic positions and isotropic temperature factors for Mg, Al/Si, and O were refined. In addition, for our final refinement based on the double-*a* α-quartz-like superstructure, the site occupancies of Mg were refined.

RESULTS AND DISCUSSION

Sample composition

TEM observation showed that the synthesized $Mg_{0.5}AlSiO_4$ sample is homogeneous and phase pure, as is consistent with the result of synchrotron XRD (see

Always consult and cite the final, published document. See http://www.minsocam.org or GeoscienceWorld

below). EDS analysis revealed the chemical formula to be $Mg_{0.51}Al_{0.97}Si_{1.02}O_4$, which can be considered identical to the nominal $Mg_{0.5}AlSiO_4$.

Framework symmetry

Based on their single-crystal XRD study, Schulz et al. (1970b) treated $MgAl_2Si_3O_{10}$, a member of the $Mg_{0.5-0.5x}Al_{1-x}Si_{1+x}O_4$ series, as a structural analogue of β-quartz. However, later theoretical modeling demonstrated that the structure of $MgAl_2Si_3O_{10}$ has a distinct, α-quartz-like character (Sternitzke and Müller 1991). More specifically, this phase may be comprised of fine α-quartz Dauphiné twins (space group $P3_221$ or $P3_121$) that are related by a two-fold rotation along the c-axis, giving the apparent β-quartz symmetry ($P6_222$ or $P6_422$). Furthermore, like α-quartz, the $Mg_{0.5-0.5x}Al_{1-x}Si_{1+x}O_4$ phases exhibit positive CTEs, in contrast with the negative CTEs of β-quartz and its derivatives such as β-$LiAlSiO_4$. Hence, in our Rietveld analyses of synchrotron XRD data, we employed both the β- and α-quartz framework models.

The results show that the α-quartz framework gave a significantly improved fit to the data; the refinement agreement parameters R_{wp}, R_p and χ^2 for the α-quartz model were 4.49%, 3.70% and 3.77, respectively, compared with R_{wp} = 4.87%, R_p = 3.96%, and χ^2 = 4.43 using the β-quartz model (Table 1). This comparison suggests that the true symmetry of $Mg_{0.5}AlSiO_4$ is trigonal with a space group of $P3_221$ or $P3_121$. Moreover, the thermal parameter of O obtained using the β-quartz model (6.8×10^{-2} Å^2) is significantly larger than that obtained using the α-quartz model (5.3×10^{-2} Å^2). This behavior implies that the $Mg_{0.5}AlSiO_4$ structure may be a statistical assembly of small Dauphiné twin domains with an α-quartz type framework, as postulated for the other stuffed-quartz derivatives $MgAl_2Si_3O_{10}$, $HAlSi_2O_6$, and $Na_{0.5}H_{0.5}AlSi_2O_6$ (Müller et al. 1990). The obtained unit-cell parameters, atomic coordinates and thermal

Always consult and cite the final, published document. See http://www.minsocam.org or GeoscienceWorld

parameters, together with selected bond lengths and bond angles, are listed in Tables 1, 2 and 3, respectively. The fitted XRD pattern is plotted in Figure 1.

Al/Si disorder

In framework aluminosilicates, [AlO_4] tetrahedra tend to connect via corner sharing with [SiO_4] tetrahedra, rather than other [AlO_4] tetrahedra, as the nearest neighbors. In other words, Al-O-Si linkages are energetically more favorable than a combination of Al-O-Al and Si-O-Si — the so-called "Al-avoidance" principle (Loewenstein 1954). The ordering of Al and Si via "Al-avoidance" has been found operative in numerous minerals such as feldspar (Ribbe 1983). In particular, for phases with Si/Al =1, including β-$LiAlSiO_4$, this principle dictates that only Al-O-Si linkages occur in their structures. As a result, the cell parameter *c* of β-$LiAlSiO_4$ is doubled relative to that of the prototype β-quartz, as evidenced by the occurrence of superlattice reflections with *h, k* = even, *l* = odd (named as *c*-reflections) (Tscherry et al. 1972; Pillars and Peacor 1973; Guth and Heger 1979; Xu et al. 1999b).

However, in crystals formed under non-equilibrium conditions such as fast quenching (and, of course, in glasses and melts), the thermodynamically unfavorable Al-Si disorder can occur, due to large kinetic barriers for Al-Si ordering. In fact, disordered phases have been synthesized in several systems, including cordierite (Putnis and Angel 1985), anorthite (Carpenter 1991; Phillips et al. 1992) and β-eucryptite (Xu et al. 1999c; Phillips et al. 2000), by crystallizing the glasses at relatively low temperatures and/or short times. Given the annealing conditions (1173 K for ~7 h) of our $Mg_{0.5}AlSiO_4$ sample, the Al/Si distribution of this phase is likely to be significantly disordered.

Figure 2 shows a ^{29}Si MAS-NMR spectrum of $Mg_{0.5}AlSiO_4$. Compared with the ^{29}Si NMR spectra for β-$LiAlSiO_4$ obtained at similar experimental conditions (Phillips et

Always consult and cite the final, published document. See http://www.minsocam.org or GeoscienceWorld

al. 2000), this profile is much broader, and the peaks due to different environments of Si are less well-resolved, suggesting a more disordered Al/Si distribution. This behavior is consistent with the absence of long-range Al/Si order, which would produce *c*-reflections (such as 201) in the synchrotron XRD pattern (Fig. 3). Nevertheless, the observed profile in Figure 2 can be deconvoluted into peaks centered at -108.5, -103.7, -100.0, -93.9, -86.9 and -78.7 ppm with relative intensities of 7.91 : 8.62 : 16.37 : 45.49 : 20.59 : 1.02 (Table 4). The full-widths at half maximum (FWHM) of these peaks are 7.4, 6.0, 6.0, 8.1, 6.0 and 6.8 ppm, respectively. For the deconvolution, we did not use any constraints on peak positions, intensities and widths. Based on ^{29}Si NMR chemical shifts of other framework aluminosilicates, we assign the peaks at -108.5, -103.7, -100.0, -93.9, and -86.9 ppm to Si atoms that have zero to four Al in the adjacent framework sites [Si(0Al), Si(1Al), Si(2Al), Si(3Al) and Si(4Al)], respectively. The small peak at -78.7 ppm (1.02% relative intensity) can be assigned to a surface Q3 site, where Si is linked to three Si or Al atoms as the next nearest neighbors.

The degree of Al/Si short-range disorder can be derived from the relative intensities of Si(*n*Al) peaks. For $Mg_{0.5}AlSiO_4$, since its Si/Al ratio equals 1, the number of Al-O-Al linkages equals the number of Si-O-Si linkages. The number of Si-O-Si linkages per Si atom (i.e., per two O atoms) ($x_{Si\text{-}O\text{-}Si}$) is calculated as: $x_{Si\text{-}O\text{-}Si} = \frac{1}{4} \sum(4\text{-}n)I_n$, where I_n is the intensity of the peak assigned to Si having n Al atoms as the next nearest neighbors, normalized to a total integrated intensity of unity. The obtained $x_{Si\text{-}O\text{-}Si}$ value is 0.218 (with the Q3 peak ignored), and thus the number of Al-O-Al linkages per two O atoms ($x_{Al\text{-}O\text{-}Al}$) is also 0.218. This value is smaller than the concentration of Al-O-Al in a statistically random distribution of Al and Si, where $x_{Al\text{-}O\text{-}Al} = 0.5$. Since $x_{Al\text{-}O\text{-}Al} = 0$ in the

Always consult and cite the final, published document. See http://www.minsocam.org or GeoscienceWorld

fully ordered Al/Si configuration, the degree of Al/Si short-range disorder in $Mg_{0.5}AlSiO_4$ is calculated to be 44% (i.e., the degree of Al/Si order = 56%). Hence, despite a strong thermodynamic driving force for Al/Si ordering, the $Mg_{0.5}AlSiO_4$ phase is significantly disordered due to kinetic hindrance in relation to reaching equilibrium. Determination of the detailed scheme for Al/Si disorder, including the configuration of linkages beyond the next nearest neighbors of Al/Si, would require NMR data (^{29}Si, ^{27}Al and ^{18}O) with higher resolution.

Mg order and superstructure

Although Al and Si are largely disordered over the framework sites of $Mg_{0.5}AlSiO_4$, Mg might exhibit positional ordering in the channels, resulting in superstructures along the **a**-axes. In fact, a number of previous XRD measurements of other Al/Si-disordered $Mg_{0.5-0.5x}Al_{1-x}Si_{1+x}O_4$ phases (such as $MgAl_2Si_3O_{10}$) revealed extensive superlattice reflections, indicating up to several tens of *a*-superperiodicities relative to the prototype quartz structure (Schulz et al. 1971b). Close inspection of our synchrotron XRD pattern of $Mg_{0.5}AlSiO_4$ did reveal extra, weak peaks indicative of doubling of the *a*-dimension compared to that of quartz (Fig.3). Following the same terminology used for the superlattice reflections of β-$LiAlSiO_4$, which shows doubled periodicities along both the **c** and **a** axes, these diffraction peaks are the so-called *a*-reflections: *h, k* = odd or *h*+*k* = odd; *l* = odd (Tscherry et al. 1972). The weak superlattice reflections are more evident in electron diffraction patterns, presumably due to dynamical diffraction. Figure 4 is a SAED pattern of $Mg_{0.5}AlSiO_4$ along [0-21], which shows distinct *a*-reflections such as 100 and 012, confirming the doubling along the **a**-axes in $Mg_{0.5}AlSiO_4$.

Always consult and cite the final, published document. See http://www.minsocam.org or GeoscienceWorld

Since our diffraction experiments, especially electron diffraction, indicate that the cell parameter *a* of $Mg_{0.5}AlSiO_4$ is doubled with respect to that of quartz, the structural parameters obtained using the prototype quartz unit-cell (Tables 1-3) represent those for an average structure. Thus we re-analyzed our synchrotron XRD data in terms of the *a*-doubled superstructure using the Rietveld method. As expected, the addition of the extra superlattice peaks (though weak) in this refinement improved the fit significantly; the refinement agreement parameters R_{wp}, R_p and χ^2 for the superstructure model were 3.87%, 3.37% and 2.81, respectively, compared with R_{wp} = 4.49%, R_p = 3.70%, and χ^2 = 3.77 using the prototype α-quartz model. The unit-cell parameters, atomic coordinates and thermal parameters, and selected bond lengths and angles for this superstructure are listed in Tables 1, 5 and 6, respectively.

As is well known, the occurrence of the doubled *a*-periodicities in β-$LiAlSiO_4$ is due to Li positional order in the channels parallel to **c**. More specifically, Li resides over alternating tetrahedral positions along the channels, and further, neighboring channels have different sets of sites occupied by Li. Analogous to β-$LiAlSiO_4$, $Mg_{0.5}AlSiO_4$ may contain two types of channels that differ in the distribution and/or concentration of Mg, causing the *a*-periodicities to double. To reveal the Mg positions in $Mg_{0.5}AlSiO_4$, we constructed difference electron Fourier (DELF) maps using the *a*-superstructure model with Mg atoms omitted (Fig. 5). The DELF syntheses revealed that the Mg atoms are located in octahedral sites with Mg-O distances ranging from 1.79(2) to 2.96(4) Å (Table 6).

This result contrasts with that of Li, which occupies the tetrahedral channel sites in β-$LiAlSiO_4$. On the other hand, an octahedral coordination for Mg is consistent with the Mg bonding environment in $MgAl_2Si_3O_{10}$ (Schulz et al. 1970b), and it also agrees

Always consult and cite the final, published document. See http://www.minsocam.org or GeoscienceWorld

with a density functional theory study of $Mg_{0.5}AlSiO_4$ (Lichtenstein et al. 2000). Moreover, Mg is disordered over all the available sites along the channels. However, the site occupancies of Mg within the neighboring channels are different: 0.263 for the central channel (0, 0) and 0.246 for three side channels (0.5, 0), (0, 0.5) and (0.5, 0.5) (Fig. 5). This difference, though small, may be coupled with differences in the Al/Si framework distortions around the two types of channels, collectively resulting in the *a*-doubled superperiodicities of $Mg_{0.5}AlSiO_4$.

Effects of channel cation on the quartz framework

The occupancy of the octahedral channel sites by Mg in $Mg_{0.5}AlSiO_4$ is in striking contrast with that of the tetrahedral sites by Li in $LiAlSiO_4$. Apparently, this disparity is responsible for the difference in the type of quartz-like framework: α-quartz for $Mg_{0.5}AlSiO_4$ and β-quartz for $LiAlSiO_4$ (Table 7). Figures 7A and 7B show the bonding environments of Li^+ and Mg^{2+} in quartz frameworks of $LiAlSiO_4$ and $Mg_{0.5}AlSiO_4$, respectively. For ease of comparison, the structures having disordered Al/Si and Li or Mg configurations are used.

In β-$LiAlSiO_4$ (Fig. 7A), each channel [LiO_4] tetrahedron shares edges with two of the [Si/AlO_4] chain tetrahedra, and the Li cations occur at the same *z* height as the Al/Si cations in those tetrahedra (Xu et al. 1999c). The Li cation is equidistant from each of the four coordinating O anions (~2.36 Å). To minimize repulsion between Li and Al/Si, the framework widens along the **a**-axes, parallel to the (001) plane (Palmer 1994), leading to a smaller *c*/*a* ratio (1.0424) compared with that of β-quartz (1.0925) (Table 7).

Within these quartz channels, the tetrahedral sites alternate with octahedrally coordinated channel sites. In the hexagonal β-quartz framework, the octahedral channel

Always consult and cite the final, published document. See http://www.minsocam.org or GeoscienceWorld

cation is situated at the same *z* height as two of the coordinating O anions. The bond distance between these two O anions and the octahedral channel cation is very short (~1.85 Å), whereas the remaining four cation-oxygen distances are much longer (>2.3 Å).

It appears that, to accommodate Mg between the two close O atoms, neighboring [Si/AlO_4] tetrahedra tilt about the **a**-axes (Fig. 7B), resulting in framework transformation from β- to α-quartz. In addition, the occupancy of Mg in an octahedral channel site effectively pushes the two close O atoms apart and attracts the other four O along the **c** axis, shortening the *c* dimension. Hence, the *c*/*a* ratio of $Mg_{0.5}AlSiO_4$ (1.0195) is significantly smaller than those of $LiAlSiO_4$ (1.0424) and β-quartz (1.0925) (Table 7).

As demonstrated in Xu et al. (1999c), changes in quartz framework dimensions occur not only via tilting of [Si/AlO_4] tetrahedra but also by individual tetrahedral deformation. Deviation of a polyhedron from regularity can be evaluated using distortion parameters, including quadratic elongation and bond angle variance (Robinson et al., 1971; Hazen and Finger 1982). Quadratic elongation, $\langle\lambda\rangle$, is defined as:

$$\langle\lambda\rangle = \sum[(l_i/l_0)^2/n] \quad (1)$$

where l_0 is the center-to-vertex distance of a regular polyhedron of the same volume, l_i is the distance from the center to the *i*th vertex (coordinating atoms) of the distorted polyhedron, and *n* is the coordination number of the central atom. The $\langle\lambda\rangle$ value for a regular polyhedron is 1, and that for a distorted polyhedron is > 1. Bond angle variance, σ^2, is defined as:

$$\sigma^2 = \sum[(\theta_i-\theta_0)^2/(n-1)] \quad (2)$$

Always consult and cite the final, published document. See http://www.minsocam.org or GeoscienceWorld

where θ_0 is the ideal bond angle for a regular polyhedron (e.g., 109.5° for a tetrahedron), θ_i is the *i*th bond angle, and *n* is the coordination number. The σ^2 value is zero for a regular polyhedron and positive for a distorted polyhedron.

As shown in Table 7, the $<\lambda>$ and σ^2 values increase, respectively, from 1.00100 and 4.22095 for β-SiO_2 to 1.00790 and 32.35479 for $LiAlSiO_4$ and to 1.01135 and 43.64646 for $Mg_{0.5}AlSiO_4$.Thus, occupancy of channel sites by Li^+ and Mg^{2+} can significantly deform neighboring [Si/AlO_4] framework tetrahedra, and further, octahedral channel Mg^{2+} has a more marked influence than tetrahedral Li^+. In particular, the degree of deformation is reflected more obviously by the bond angle variance σ^2. This is reasonable, given that the effects of channel cations lie mainly on expanding the [Si/AlO_4] tetrahedra parallel to (001) and, concomitantly, contracting them along **c**. Since each channel octahedron has two closely spaced O atoms at similar *z* heights (Fig. 7B), Mg^{2+} exerts more pronounced effects on the host framework than does Li^+.

IMPLICATIONS

Framework aluminosilicates are important phases in natural rocks and in synthetic ceramic/composite materials. Extra-framework cations situated in channels and/or cavities may exert significant effects on framework topologies, to the point of inducing "morphotropic" phase transitions that are stimulated by composition rather than temperature or pressure (Heaney 2000). This study demonstrates the different responses of the quartz framework to the extra-framework occupancy of Mg^{2+} and Li^+ within the channel sites. The presence of Mg^{2+} within the octahedral channel site, rather than the tetrahedral site associated with Li^+, transforms the structure from β- to α-quartz-like, and this distortion results in dramatically different thermal expansion properties. This

Always consult and cite the final, published document. See http://www.minsocam.org or GeoscienceWorld

information can be used to synthesize stuffed-quartz derivatives with tailored expansion behaviors, and the general properties documented here may be extrapolated to other framework phases.

ACKNOWLEDGMENTS

We are grateful to Michael Carpenter and an anonymous reviewer for their helpful comments. We thank David Cox for assistance with synchrotron XRD experiments. The experiments were carried out at the National Synchrotron Light Source (NSLS), Brookhaven National Laboratory, which was supported by the U.S. Department of Energy, Office of Science, Office of Basic Energy Sciences, under Contract No. DE-AC02-98CH10886. We also acknowledge NSF grant #EAR11-47728 and support from the laboratory-directed research and development (LDRD) program of Los Alamos National Laboratory, which is operated by Los Alamos National Security LLC, under DOE Contract DE-AC52-06NA25396.

Always consult and cite the final, published document. See http://www.minsocam.org or GeoscienceWorld

REFERENCES CITED

Beall, G.H. (1994) Industrial applications of silica. In Mineralogical Society of America Reviews in Mineralogy, 29, 468-505.

Buerger, M.J. (1954) The stuffed derivatives of the silica structures. American Mineralogist, 39, 600-614.

Carpenter, M.A. (1991) Mechanisms and kinetics of Al-Si ordering in anorthite: I. Incommensurate structure and domain coarsening. American Mineralogist, 76, 1110-1119.

Cox, D.E., Toby, B.H., and Eddy, M.M. (1988) Acquisition of powder diffraction data with synchrotron radiation. Australian Journal of Physics, 41, 117-131.

Finger, L.W., Cox, D.E., and Jephcoat, A.P. (1994) A correction for powder diffraction peak asymmetry due to axial divergence. Journal of Applied Crystallography, 27, 892-900.

French, B.M., Jezek, P.A., and Appleman, D.E. (1978) Virgilite – new lithium aluminum silicate mineral from Macusani glass, Peru. American Mineralogist, 63, 461-465.

Ghiorso, M.S., Carmichael, I.S.E., and Moret, L.K. (1979) Inverted high-temperature quartz. Contributions to Mineralogy and Petrology, 68, 307-323.

Guth, H. and Heger, G. (1979) Temperature dependence of the crystal structure of the one-dimensional Li^{+}-conductor β-eucryptite ($LiAlSiO_4$). In P. Vashista, J.N. Mundy and G.K. Shenoy, Eds., Fast ion transport in solids, p. 499-502. Elsevier North Holland, New York.

Always consult and cite the final, published document. See http://www.minsocam.org or GeoscienceWorld

Hazen, R.M. and Finger, L.W. (1982) Comparative Crystal Chemistry: Temperature, Pressure, Composition and the Variation of Crystal Structure. John Wiley & Sons, New York.

Heaney, P.J. (2000) Phase transformations induced by solid solution. In Mineralogical Society of America Reviews in Mineralogy and Geochemistry, 39, 135-174.

Keith, M.L. and Tuttle, O.F. (1952) Significance of variance in high-low inversion of quartz. American Journal of Science, 253a, 203-280.

Larson, A.C. and Von Dreele, R.B. (2000) GSAS–General Structure Analysis System. Los Alamos National Laboratory Report No. LAUR 86-748, 179 p.

Lichtenstein, A.I., Jones, R.O., de Gironcoli, S., and Baroni, S. (2000) Anisotropic thermal expansion in silicates: A density functional study of β-eucryptite and related materials. Physical Review B, 62, 11487-11493.

Loewenstein, W. (1954) The distribution of aluminum in the tetrahedra of silicates and aluminates. American Mineralogist, 39, 92-96.

Müller, G. (1995) The scientific basis. In H. Bach, Ed., Low thermal expansion glass ceramics, p. 13–49. Springer-Verlag, Berlin.

Müller, G., Hoffmann, M., and Neeff, R. (1988) Hydrogen substitution in lithium-aluminosilicates. Journal of Materials Science, 23, 1779-1785.

Müller, G., Paulus, H., and Darmstadt, J.S. (1990) Synthesis and structure of β-quartz type $Na_{0.5}H_{0.5}AlSi_2O_6$ as compared to $LiAlSi_2O_6$. N. Jb. Miner. Mh., H11, 493-503.

Palmer, D.C. (1994) Stuffed derivatives of the silica polymorphs. In Mineralogical Society of America Reviews in Mineralogy, 29, 83-122.

Always consult and cite the final, published document. See http://www.minsocam.org or GeoscienceWorld

Petzoldt, J. (1967) Metastabile mischkristalle mit quarzstruktur mit oxidsystem Li_2O-MgO-ZnO-Al_2O_3-SiO_2. Glastechnische Berichte, 40, 385-396.

Paulus, H., Fuess, H., Müller, G., Darmstadt, J.S., and Vogt, T. (1990) The crystal structure of β-quartz type $HAlSi_2O_6$. N. Jb. Miner. Mh., H5, 232-240.

Phillips, B.L., Kirkpatrick, R.J., and Carpenter, M.A. (1992) Investigation of short range Al,Si order in synthetic anorthite by ^{29}Si MAS NMR spectroscopy. American Mineralogist, 77, 484-494.

Phillips, B.L., Xu, H., Heaney, P.J., and Navrotsky, A. (2000) ^{29}Si and ^{27}Al MAS-NMR spectroscopy of β-eucryptite ($LiAlSiO_4$): The enthalpy of Si,Al ordering. American Mineralogist, 85, 181-188.

Pillars, W.W. and Peacor, D.R. (1973) The crystal structure of beta eucryptite as a function of temperature. American Mineralogist, 58, 681-690.

Putnis, A. and Angel R.J. (1985) Al,Si ordering in cordierite using "Magic Angle Spinning" NMR. II: Models of Al,Si order from NMR data. Physics and Chemistry of Minerals, 12, 217-222.

Ramalingam, S. and Reimanis, I.E. (2012) Effect of doping on the thermal expansion of β-eucryptite prepared by sol-gel methods. Journal of the American Ceramic Society, 95, 2939-2943.

Ribbe, P.H. (1983) Aluminum-silicon order in feldspars: Domain textures and diffraction patterns. In Mineralogical Society of America Reviews in Mineralogy, 2, 21-55.

Robinson, K., Gibbs, G.V., and Ribbe, P.H. (1971) Quadratic elongation: A quantitative measure of distortion in coordination polyhedral. Science, 172, 567-570.

Always consult and cite the final, published document. See http://www.minsocam.org or GeoscienceWorld

Roy, R. (1995) Low thermal expansion ceramics: A retrospective. In: Stinton and Limaye (eds.), Low-expansion materials, Ceramic Transactions, Vol. 52, The American Ceramic Society, 1-4.

Schreyer, W. and Schairer, J.F. (1961) Metastable solid solution with quartz-type structure on the join SiO_2-$MgAl_2O_4$. Zeitschrift für Kristallographie, 116, 60-82.

Schulz, H. (1971) Influence of heat-treatment on the average structure of $Mg[Al_2Si_3O_{10}]$, a stuffed derivative of the high-quartz structure. Zeitschrift für Kristallographie, Bd. 134, S. 253-261.

Schulz, H., Muchow, G.M., Hoffmann, W., and Bayer, G. (1971a) X-ray study of Mg-Al silicate high-quartz phases. Zeitschrift für Kristallographie, Bd. 133, S. 91-109.

Schulz, H., Hoffmann, W., and Muchow, G.M. (1971b) The average structure of $Mg[Al_2Si_3O_{10}]$, a stuffed derivative of the high-quartz structure. Zeitschrift für Kristallographie, Bd. 134, S. 1-27.

Smith, J.V. and Steele, I.M. (1984) Chemical substitution in silica polymorphs. Neues Jahrbuch für Mineralogie Monatschefte, 3, 137-144.

Sternitzke, M. and Müller, G. (1991) Crystal structure and thermal expansion of quartz-type aluminosilicates. Journal of Materials Science, 26, 3051-3056.

Strnad, Z. (1986) Glass-Ceramic Materials. Glass Science and Technology, Vol. 8. Elsevier, Amsterdam.

Thompson, P., Cox, D.E., and Hastings, J. (1987) Rietveld refinement of Debye-Scherrer synchrotron X-ray data for Al_2O_3. Journal of Applied Crystallography, 20, 79-83.

Always consult and cite the final, published document. See http://www.minsocam.org or GeoscienceWorld

Tscherry, V., Schulz, H., and Laves, F. (1972) Average and super structure of β-eucryptite ($LiAlSiO_4$), Part II, Superstructure. Zeitschrift für Kristallographie, 135, 175-198.

Will, G., Bellotto, M., Parrish, W., and Hart, M. (1988) Crystal structures of quartz and magnesium germanate by profile analysis of powder diffractometer data. Journal of Applied Crystallography, 21, 182-191.

Wright, A.F. and Lehmann, M.S. (1981) The structure of quartz at 25 and 500 °C determined by neutron diffraction. Journal of Solid State Chemistry, 36, 371-380.

Xu, H., Heaney, P.J., Navrotsky, A., Topor, L., and Liu, J. (1999a) Thermochemistry of stuffed quartz-derivative phases along the join LiAlSiO4-SiO2. American Mineralogist, 84, 1360-1369.

Xu, H., Heaney, P.J., and Böhm, H. (1999b) Structural modulations and phase transitions in β-eucryptite: An in-situ TEM study. Physics and Chemistry of Minerals, 26, 633-643.

Xu, H., Heaney, P.J., Yates, D.M., Von Dreele, R.B., and Bourke, M.A. (1999c) Structural mechanisms underlying near-zero thermal expansion in β-eucryptite: A combined synchrotron X-ray and neutron Rietveld analysis. Journal of Materials Research, 14, 3138-3151.

Xu, H., Heaney, P.J., and Beall, G.H. (2000) Phase transitions induced by solid solution in stuffed derivatives of quartz: A powder synchrotron XRD study of the $LiAlSiO_4$-SiO_2 join. American Mineralogist, 85, 971-979.

Xu, H., Heaney, P.J., and Navrotsky, A. (2001) Thermal expansion and structural transformations of stuffed derivatives of quartz along the $LiAlSiO_4$-SiO_2 join: A

Always consult and cite the final, published document. See http://www.minsocam.org or GeoscienceWorld

variable-temperature powder synchrotron XRD study. Physics and Chemistry of Minerals, 28, 302-312.

Table 1 Unit-cell constants and refinement agreement parameters of $Mg_{0.5}AlSiO_4$

Structure model	a (Å)	c (Å)	V (Å^3)	χ^2	R_{wp}(%)	R_p(%)
$P6_222$	5.21986(8)	5.3215(1)	125.569(4)	4.43	4.87	3.96
$P3_221$	5.21978(7)	5.3215(1)	125.565(4)	3.77	4.49	3.70
$P3_221$/superstructure	10.4396(2)	5.3214(1)	502.26(2)	2.81	3.87	3.37

Table 2 Atomic coordinates and atomic thermal parameters of $Mg_{0.5}AlSiO_4$ in the basic α-quartz model (space group $P3_221$)

Atom	x	y	z	U_{iso} [1)]
Mg	0.027(3)	0	1/6	4.1(3)
Si/Al	0.4901(8)	0	2/3	1.81(4)
O	0.5909(5)	0.7781(9)	0.8025(9)	5.3(2)

1) The unit of U_{iso} is Å^2/100.

Always consult and cite the final, published document. See http://www.minsocam.org or GeoscienceWorld

Table 3 Selected bond distances (Å) and bond angles (º) of $Mg_{0.5}AlSiO_4$ in the basic α-quartz model (space group $P3_221$)

MgO_6 octahedron		Si/AlO_4 tetrahedron	
Mg-O[1)]	2.765(9)	Si/Al-O[1)]	1.659(4)
	2.360(11)		1.628(4)
	1.871(3)	O-Si/Al-O	109.9(2)[2)]
O-Mg-O	119.6(4)[2)]		113.96(4)[2)]
	70.4(4)[2)]		96.4(3)
	100.8(7)		112.0(4)
	165.7(10)	Si/Al-O-Si/Al	147.7(2)

1) Each value corresponds to two edges; 2) Each value corresponds to two angles.

Table 4 Relative intensities of ^{29}Si NMR peaks obtained from least-squares fitting of the spectrum (Fig. 2) to a sum of Gaussian curves

Site	Position (ppm)	FWHM[1)] (ppm)	Intensity (%)
Q3	-78.7	6.8	1.02
Si(4Al)	-86.9	6.0	20.59
Si(3Al)	-93.9	8.1	45.49
Si(2Al)	-100.0	6.0	16.37
Si(1Al)	-103.7	6.0	8.62
Si(0Al)	-108.5	7.4	7.91

1) Full width at half maximum.

Always consult and cite the final, published document. See http://www.minsocam.org or GeoscienceWorld

Table 5 Atomic coordinates and thermal parameters of $Mg_{0.5}AlSiO_4$ in the α-quartz superstructure model with doubled **a**-axes (space group $P3_221$)

Atom[1)]	*x*	*y*	*z*	U_{iso}[2)]
Mg1	-0.008(5)	0	1/6	3.9(3)
Mg2	0.488(6)	0	1/6	3.9(3)
Mg3	0.489(4)	0.504(5)	0.117(4)	3.9(3)
T1	0.254(2)	0	2/3	1.99(3)
T2	0.760(1)	0	2/3	1.99(3)
T3	0.254(2)	0.502(1)	0.663(2)	1.99(3)
O1	0.193(2)	0.111(2)	0.767(3)	4.3(2)
O2	0.693(2)	0.089(2)	0.848(3)	4.3(2)
O3	0.220(1)	0.604(3)	0.830(4)	4.3(2)
O4	0.708(2)	0.613(2)	0.794(4)	4.3(2)

1) T = Al, Si; 2) The unit of U_{iso} is $Å^2/100$; the U_{iso} values of like atoms are constrained to be equal.

Always consult and cite the final, published document. See http://www.minsocam.org or GeoscienceWorld

Table 6 Selected bond distances (Å) and bond angles (º) of $Mg_{0.5}AlSiO_4$ in the α-quartz superstructure model with doubled **a**-axes (space group $P3_221$)[1)]

$Mg1O_6$ octahedron[2)]			$T1O_4$ tetrahedron[2)]	
Mg1-O1	2.80(4)		T1-O1	1.67(2)
	2.20(4)		T1-O4	1.65(2)
	1.80(2)			
			$T2O_4$ tetrahedron[2)]	
$Mg2O_6$ octahedron[2)]			T2-O1	1.71(2)
Mg2-O2	2.52(4)		T2-O2	1.71(2)
Mg2-O3	1.99(2)			
Mg2-O4	2.36(4)		$T3O_4$ tetrahedron	
			T3-O2	1.68(2)
$Mg3O_6$ octahedron			T3-O3	1.56(2)
Mg3-O2	1.81(4)		T3-O3	1.62(3)
Mg3-O2	2.30(4)		T3-O4	1.62(2)
Mg3-O3	2.74(4)			
Mg3-O3	2.95(4)		T-O-T angles	
Mg3-O4	2.62(4)		T1-O1-T2	136.0(10)
Mg3-O4	1.92(4)		T2-O2-T3	142.4(10)
			T3-O3-T3	159.6(11)
			T1-O4-T3	148.1(14)

1) T = Si, Al.

2) Each value corresponds to two edges.

Always consult and cite the final, published document. See http://www.minsocam.org or GeoscienceWorld

Table 7 Structural comparison between β-SiO_2, $LiAlSiO_4$ and $Mg_{0.5}AlSiO_4$

Phase	Space group	Li^+ or Mg^{2+} coordination	a (Å)	c (Å)	c/a	Unit cell V (Å^3)	Tetrahedral V (Å^3)	$\langle\lambda\rangle$	σ^2
β-SiO_2[1)]	$P6_222$	N/A	4.9977	5.4601	1.0925	118.11	2.05777	1.00100	4.22095
$LiAlSiO_4$[2)]	$P6_222$	tetrahedral	5.27102(7)	5.4946(1)	1.0424	132.207(5)	2.34376	1.00790	32.35479
$Mg_{0.5}AlSiO_4$	$P3_221$	octahedral	5.21978(7)	5.3215(1)	1.0195	125.565(4)	2.23989	1.01135	43.64646

1) From Wright and Lehman (1981); 2) From Xu et al. (1999c)

Always consult and cite the final, published document. See http://www.minsocam.org or GeoscienceWorld

Figure captions

Fig. 1 Fitted synchrotron XRD pattern of $Mg_{0.5}AlSiO_4$ based on the basic α-quartz structure model (space group $P3_221$). Data are shown as plus signs, and the solid curve is the best fit to the data. Tick marks below the pattern show the positions of allowed reflections, and the lower curve represents the difference between the observed and calculated profiles. The inset shows the details of the profile from 15˚ to 38˚ 2θ.

Fig. 2 Observed and simulated ^{29}Si MAS-NMR spectra of $Mg_{0.5}AlSiO_4$. The simulated spectrum was obtained by deconvolution of the observed spectrum into components for Si(0Al), Si(1Al), Si(2Al), Si(3Al), Si(4Al) and surface Q3 sites.

Fig. 3 Expanded synchrotron XRD pattern of $Mg_{0.5}AlSiO_4$ from 6˚ to 15˚ 2θ showing occurrence of the superlattice *a*-reflection, 112, but not *c*-reflection, 201. Note that the peaks are indexed based on a doubled-*a* and doubled-*c* supercell.

Fig. 4 Selected-area electron diffraction (SAED) pattern along the [0-21] zone-axis of $Mg_{0.5}AlSiO_4$. Note that the spots are indexed based on a doubled-*a* and doubled-*c* supercell.

Fig. 5 Difference electron Fourier map along the **a**-**c** plane of $Mg_{0.5}AlSiO_4$ showing the positions of Mg^{2+} in the structure channels. Contours are drawn from 1.1 to 3.2 $e^-/Å^3$ with an interval of 0.3 $e^-/Å^3$. Note that the site occupancy of Mg^{2+} in the central channel is higher than that in the side channels.

Always consult and cite the final, published document. See http://www.minsocam.org or GeoscienceWorld

598 Fig. 6 Structure of $Mg_{0.5}AlSiO_4$ projected along (A) [001] and (B) [100].
599 Tetrahedra represent [Si/AlO_4] units, and spheres represent Mg cations.
600 Solid lines outline the *a*-doubled supercell, which is four times that of the
601 primary quartz cell.
602 Fig. 7 Coordination environments of (A) channel Li^+ in the β-quartz framework
603 of $LiAlSiO_4$ and (B) Mg^{2+} in the α-quartz framework of $Mg_{0.5}AlSiO_4$. For
604 ease of comparison, the structures are drawn based on disordered Al/Si
605 and Li or Mg configurations. Tetrahedra represent [Si/AlO_4] units, and
606 spheres represent Li^+ or Mg^{2+}.
607
608
609

Always consult and cite the final, published document. See http://www.minsocam.org or GeoscienceWorld

610

611

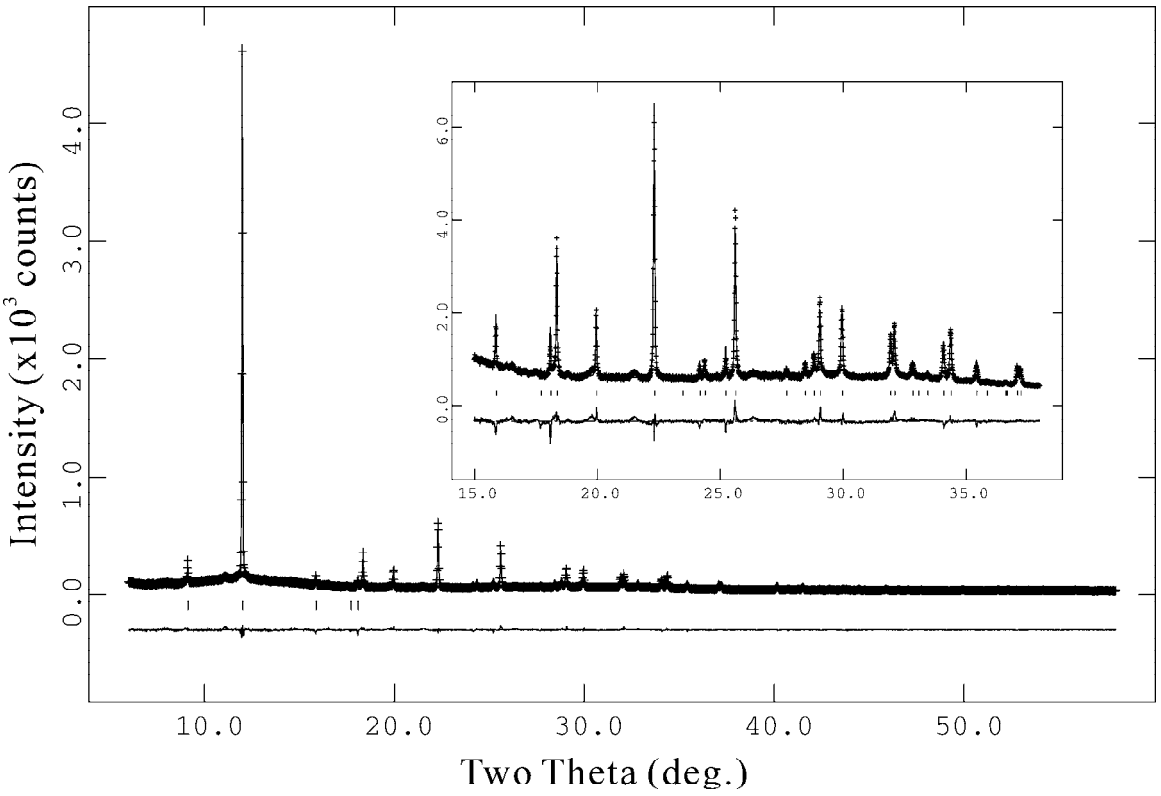

612

613

614

615 Fig. 1

Always consult and cite the final, published document. See http://www.minsocam.org or GeoscienceWorld

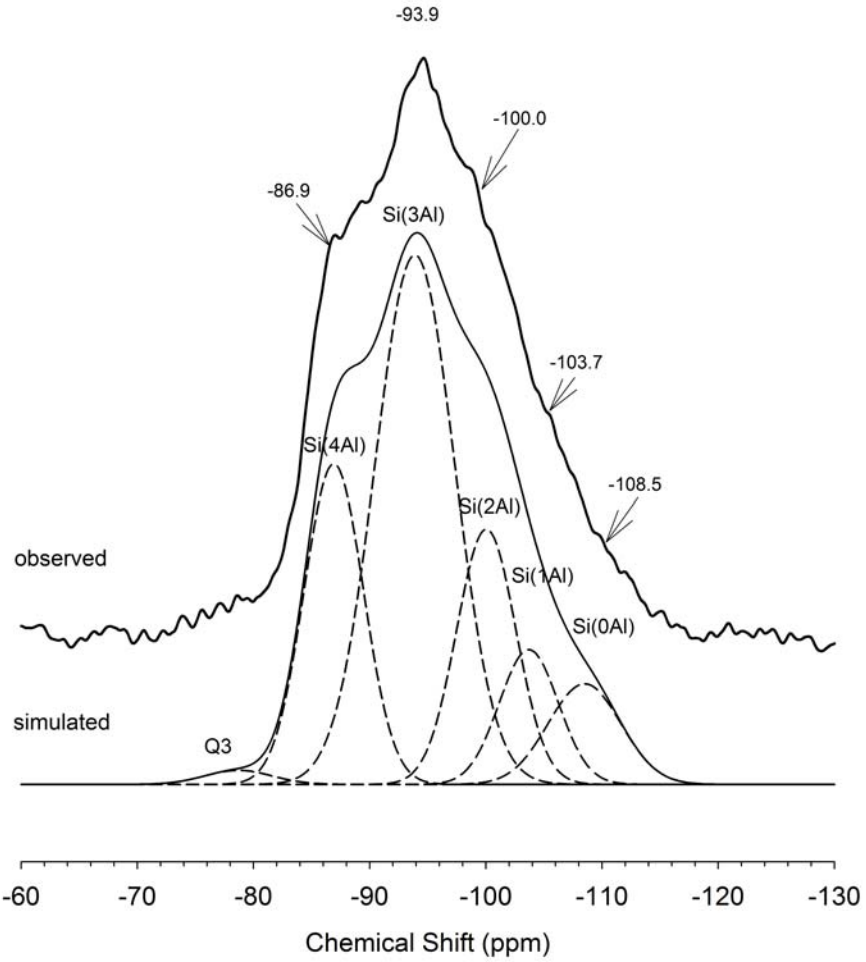

Fig. 2

Always consult and cite the final, published document. See http://www.minsocam.org or GeoscienceWorld

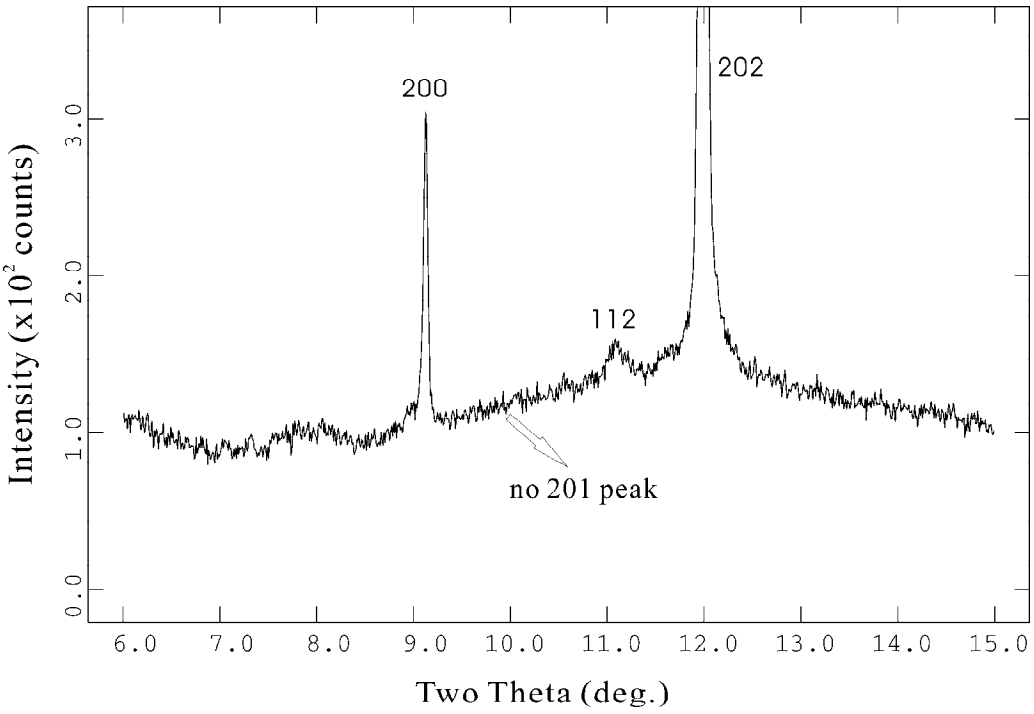

620

621 Fig. 3
622

Always consult and cite the final, published document. See http://www.minsocam.org or GeoscienceWorld

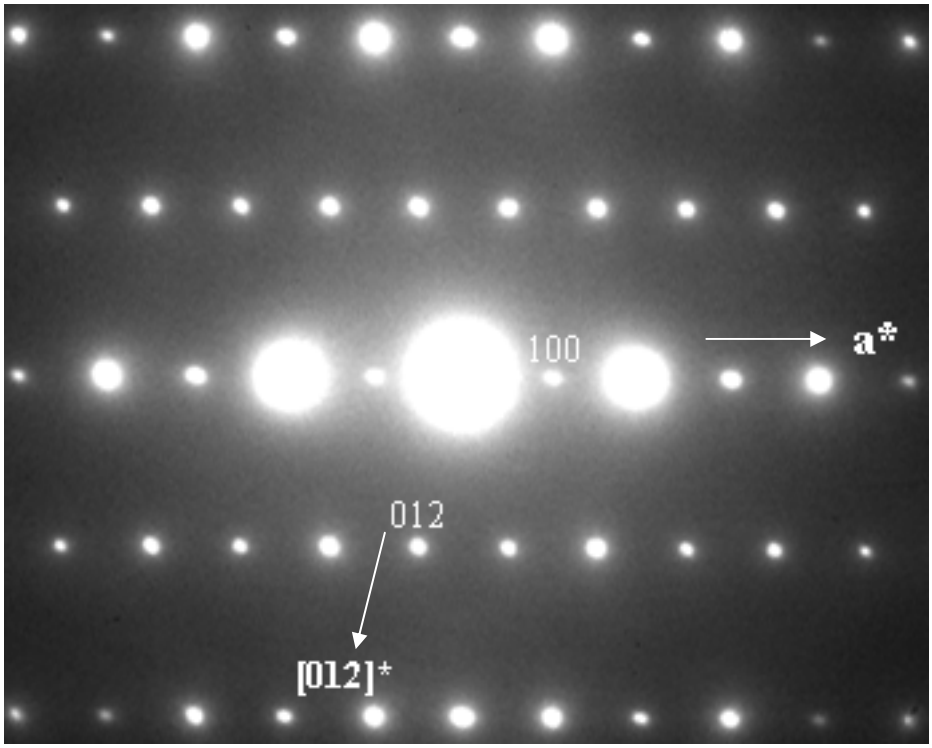

623

624 Fig. 4

625

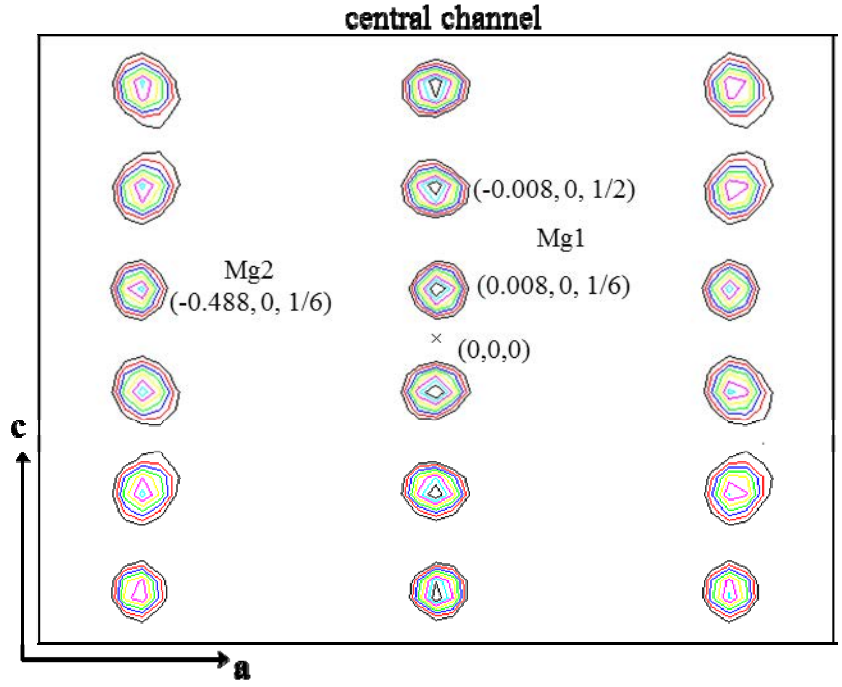

626

627 Fig. 5

Always consult and cite the final, published document. See http://www.minsocam.org or GeoscienceWorld

628

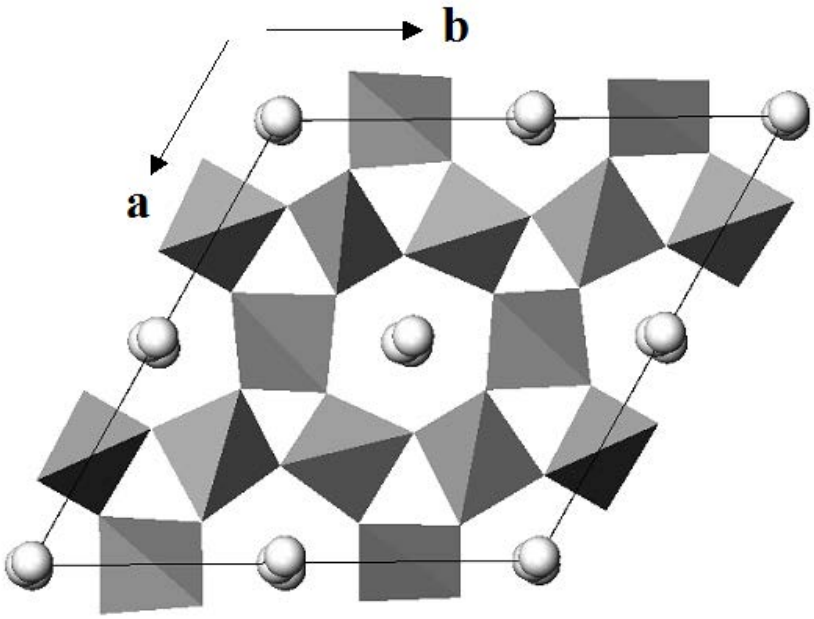

629

630 Fig. 6A

631

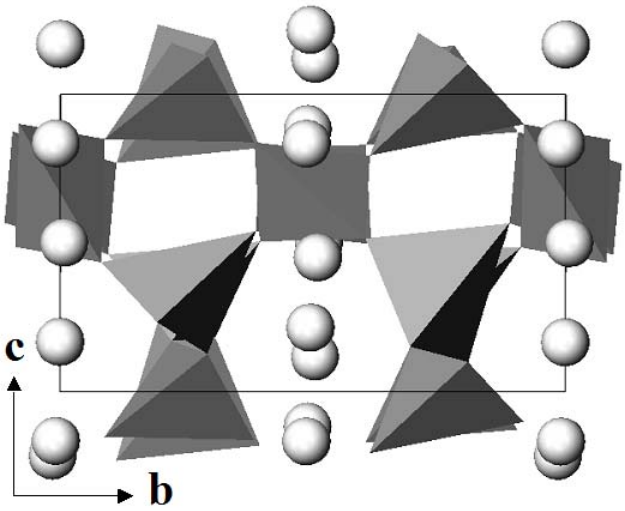

632

633 Fig. 6B

634

Always consult and cite the final, published document. See http://www.minsocam.org or GeoscienceWorld

635

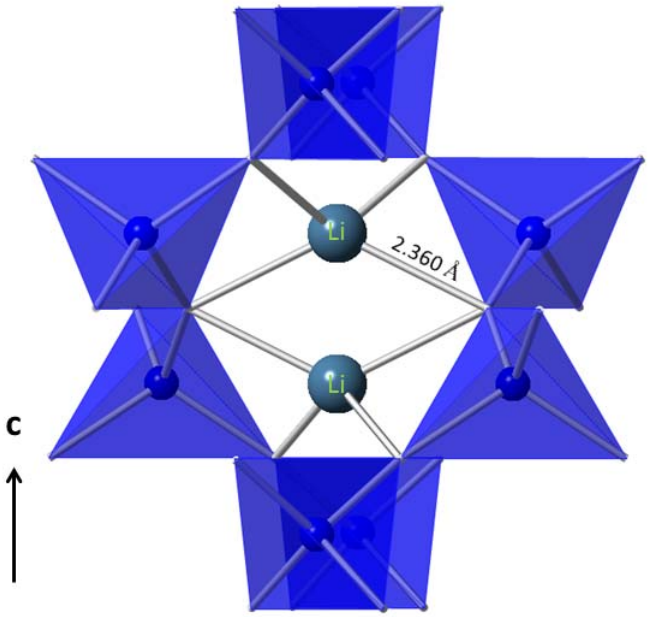

636

637 Fig. 7A

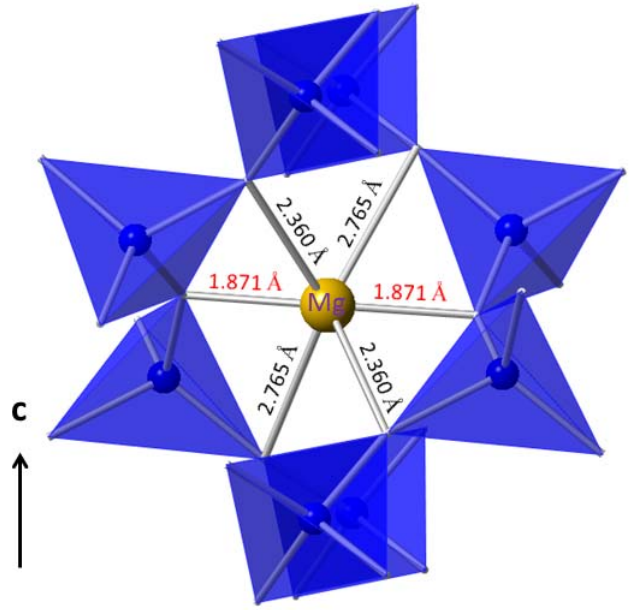

638

639 Fig. 7B

Always consult and cite the final, published document. See http://www.minsocam.org or GeoscienceWorld